ISIJ International, Vol. 58 (2018), No. 6, pp. 1155–1161

Influence of Deformability of Retained Austenite on Martensitic Transformation in Tension for Low Alloy Steel at Low Temperatures

Takayuki YAMASHITA,[1)]* Norimitsu KOGA[2)] and Osamu UMEZAWA[2)]

1) Graduate School of Engineering, Yokohama National University, 79-5 Tokiwadai, Hodogaya, Yokohama, 240-8501 Japan.
2) Faculty of Engineering, Yokohama National University, 79-5 Tokiwadai, Hodogaya, Yokohama, 240-8501 Japan.

(*Received on January 17, 2018; accepted on March 23, 2018*)

The tensile properties and mechanical stability of retained austenite in a low alloy steel were evaluated at low temperatures. Transformation-induced plasticity introduced a good balance of strength and ductility at the temperatures from 193 K to 293 K. A high work-hardening rate in the initial stage of deformation and strengthening of the ferrite matrix by lowering the temperature were responsible for the good balance. The higher work-hardening rate at low temperatures was enhanced by the stress-induced transformation of retained austenite. At 0.1 strain over a temperature range from 193 K to 293 K, the retained austenite near a zone normal to $<111>$ was mechanically stable, where not only mechanical stability but also deformability in the retained austenite and austenite grain rotation with ferrite matrix strongly affected the martensitic transformation in the steel. On the other hand, at 77 K, almost all of the retained austenite was transformed to martensite regardless of its orientation because of its low phase stability.

KEY WORDS: transformation-induced plasticity; phase stability; work hardening; retained austenite; low alloy steel.

1. Introduction

Transformation-induced plasticity (TRIP) in low alloy steel results in a good balance of strength and ductility due to deformation-induced transformation of retained austenite (γ).[1,2)] TRIP strongly depends on the mechanical stability of retained austenite, which is closely related to the testing temperature[3)] and carbon content[4)] as well as the morphology[5)] and precipitation site[6)] of the retained austenite. The role of retained austenite on strain hardening in TRIP steel was pointed out as (1) compressive long range internal stress in the ferrite (α) matrix owing to non-transformed retained austenite and other hard secondary phases (bainite and martensite), and (2) martensite hardening and stress relaxation (or plastic relaxation) by the strain-induced transformation of retained austenite.[7)] Tirumalasetty *et al.*[6)] distinguished individual retained austenite into three types: type A: austenite grains at the grain boundaries of ferrite, type B: twinned austenite grains and type C: austenite grains embedded in ferrite grains. They clarified that type C austenite was the most stable against the martensitic transformation. This is due to the fact that straining leads to a rotation of the harder retained austenite grain within the softer ferrite matrix before the austenite transforms into martensite. Thus, the rotation of individual austenite grains is also a significant factor contributing to the ductility. However, the effect of the crystal orientation on the retained austenite stability has not been analyzed. Furthermore, the transformation behavior of individual retained austenite grains at a low temperature has not been elucidated yet, although many studies have been conducted on both mechanical properties of TRIP steels and stability of retained austenite at temperatures above the room temperature.

In the present study, the tensile properties and mechanical stability of retained austenite in a low alloy steel, *i.e.* Fe-0.31C-1.74Si-1.49Mn (in mass%), have been evaluated at low temperatures. The steel exhibited a good balance of strength and ductility at 193 K.[8)] Since the balance depends on the high work-hardening rate in the early stage of deformation (below 0.1 strain) and the strengthening of the ferrite matrix by lowering the temperature, the mechanical stability of retained austenite may strongly affect martensitic transformation and high work-hardening rate in the steels. Here, the role of retained austenite on work-hardening and transformation behavior in a low alloy steel was elucidated, with an emphasis on the stability and rotation of the crystal orientation in retained austenite.

2. Experimental Procedure

2.1. Material

A 0.31C-1.74Si-1.49Mn (in mass%) steel plate was cold-rolled and annealed at 1 063 K for 400 sec in the $\alpha+\gamma$ region, and then austempered at 673 K for 600 sec.[8)] The initial volume fraction of the retained austenite was 17.2%

* Corresponding author: E-mail: yamashita-takayuki-yz@ynu.jp
DOI: http://dx.doi.org/10.2355/isijinternational.ISIJINT-2018-033

according to results of X-ray diffraction (XRD) with Cu–Kα radiation and its carbon content was calculated to be 1.32 mass% using Eq. (1).[9]

$$a_\gamma = (0.3553 \pm 0.0001) + (0.00105 \pm 0.00002)C\ (\text{at\%}) \cdots (1)$$

2.2. Tensile Tests

The configuration of tensile test specimens is shown in **Fig. 1**. Sheet-type specimens with a gauge length of 30 mm, width of 4 mm and thickness of 2.5 mm were cut using a wire cut electric discharge machine, where the longitudinal direction was parallel to the rolling direction (RD). The specimens' surface was ground using SiC emery paper of 800 grid to 2 400 grid, and was electropolished in a stirred solution of perchloric acid and ethanol at 253 K and 31 V for 30 s.

The tensile, interrupted and cyclically unloaded tests were carried out with an initial strain rate of 2.8×10^{-4} s^{-1} using a mortar-driven tensile test machine at 293 K (in air), 233 K (immersed in a cooling alcohol), 193 K (immersed in a cooling alcohol), and 77 K (immersed in liquid nitrogen). The test specimens were kept in the coolant at each temperature for 1 hour before the tests. The interrupted tests were chosen as 0.01, 0.03, 0.05 and 0.1 of the total elongation (measured with a strain gauge) as shown in **Fig. 2**. After the interrupted tests, the homogenously deformed areas in the gauge length of the specimens were cut off from the tested specimens, and were ground with the thickness of 0.5 mm to 1 mm from the surface, in order to analyze the volume of retained austenite in the specimen interior by the electron back-scatter diffraction (EBSD). The cyclically unloaded tests as shown in Fig. 2 were carried out in steps of 0.04 nominal strain up to a total of 0.12 nominal strain at 193 K and 293 K in order to analyze the transformation behavior of retained austenite in the same region on the specimen surface under each strain.

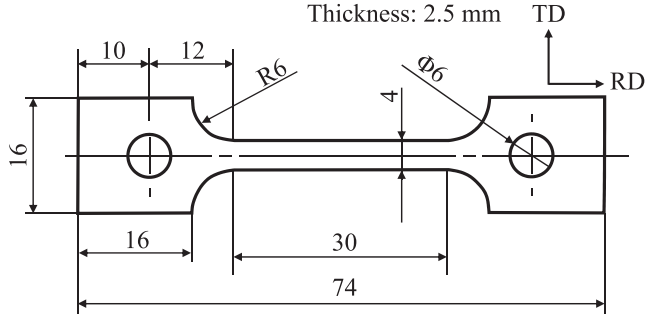

Fig. 1. Configuration of the tensile test specimen in the present study.

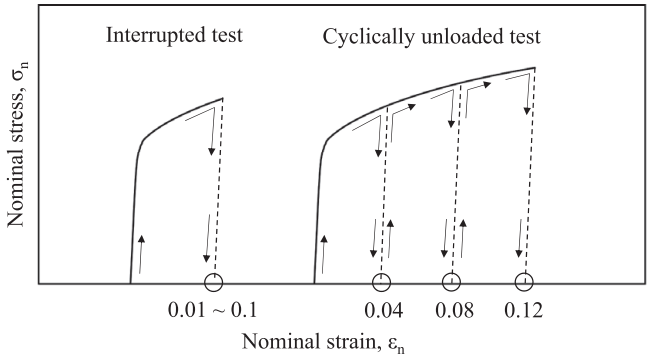

Fig. 2. Schematic illustration of interrupted test and cyclically unloaded test.

2.3. Crystal Orientation Analysis and Phase Identification

The EBSD technique with a field-emission gun scanning electron microscope was employed to analyze the retained austenite in the homogeneous deformation region on the specimen surface in both the transverse direction (TD) and normal direction (ND) for cyclically unloaded tests. Data were recorded on an area of 47 μm × 47 μm with a beam scanning step of 50 nm. Data points with a confidence index (CI) less than 0.1 were omitted as noise.

The time-of-flight neutron diffraction measurements, using iMATERIA (beamline BL20, MLF/J-PARC, Japan)[10] were also conducted to determine the volume and orientation of the retained austenite. The measurements were carried out using a sample holder for the sheet material with length of 60 mm, width of 9 mm and thickness of 2.5 mm. The homogenous deformation areas of 15 mm in length were cut off from the specimen interrupted at 0.1 strain and the fractured specimen under 0.29 strain at 293 K, respectively. Three kinds of test samples, *i.e.* the test material (non-deformed) and those homogenous deformation areas, were put into a vanadium pipe with diameter of 6 mm and were analyzed. The incident beam slit size, *i.e.* the beam spot size, was 20 mm × 20 mm. The proton beam power of the spallation neutron source was 150 kW, and the irradiation time was either 1 800 s for deformed specimens or 900 s for non-deformed ones. Rietveld texture analysis using MAUD which was described in the reference[10] was applied to the evaluation of retained austenite.

3. Results and Discussion

3.1. Microstructure

Figure 3 shows the microstructure of the test steel plate on the TD plane. The microstructure consists of a ferrite matrix, retained austenite, and bainite, as shown in Fig. 3(a). The retained austenite grains are distributed as island-, plate- or block-like areas in both the ferrite matrix and bainite regions as shown in Fig. 3(b). The initial volume fraction of the retained austenite is approximately 16.9% as determined by EBSD analysis which is in good agreement with the value obtained by XRD. The volume fraction of the retained austenite extracted from the neutron diffraction measurement is 20.4%, which is higher than the values obtained by EBSD and XRD. Since neutron diffraction measurements have a higher spatial resolution than XRD and EBSD, rather fine or thin austenite grains can be detected. The retained austenite grains satisfy the Kurdjumov-Sachs orientation relationship (K-S OR),[11] *i.e.* $(111)\gamma//(110)\alpha$ and $[1\bar{1}0]\gamma//[1\bar{1}1]\alpha$, with both ferrite and bainite matrix. Details of the orientation relationship are described in the section 3.4.

3.2. Tensile Properties

The nominal stress-strain curves at each test temperature are presented in **Fig. 4**, and their tensile properties are summarized in **Table 1**. The test steel exhibited a good balance of high tensile strength and high ductility at the temperatures

of 193 K, 233 K, and 293 K. However, early fracture was revealed at 77 K. The tensile strength increased and yield stress decreased as the temperature was lowered from 293 K to 193 K. The TRIP of the metastable austenitic steel shows an inverse temperature dependence of the yield stress as it reaches martensite start temperature (*Ms*).[12] Thus, the deformation-induced transformation may be promoted due to decrease in the stability of the retained austenite as the temperature is decreased. However, the volume fraction of the retained austenite did not decrease around the yield stress level at 193 K and 233 K as well as 0.01 strain at 293 K as determined by EBSD measurements. The martensitic transformation of retained austenite in a TRIP steel was detected at around 0.2% proof stress (lower than the yield stress of retained austenite) at 293 K using in-situ neutron diffraction.[13] Such a small amount of change in the retained austenite fraction can hardly be detected by EBSD. No martensitic transformation was detected by EBSD for the material cooled down to 193 K, either. The *Ms* temperature of retained austenite in the test steel was estimated to be 258.5 K by the Eq. (2),[14]

$$Ms = 550 - (360 \times \%C) - (40 \times \%Mn) - (0 \times \%Si) \quad \cdots (2)$$

where %C and %Mn represent carbon and manganese concentrations (mass%), respectively. The manganese concentration was assumed to be 1.5 times of the chemical content.[15,16] Although the *Ms* is for reference, the true *Ms* of the retained austenite concentrated carbon by austempering can be estimated between 77 K and 293 K. Therefore, the inverse temperature dependence of the yield stress in the temperature range between 293 K and 193 K may be explained by the promoted martensitic transformation due to the decrease in the stability of austenite as the temperature is decreased.

Figure 5 represents the relationship between the work-hardening rate and the true strain curves at each test temperature. The work-hardening rate increases as the temperature is decreased. The hardening rate of a crystal may be divided into distinct stages, typically three stages, labeled

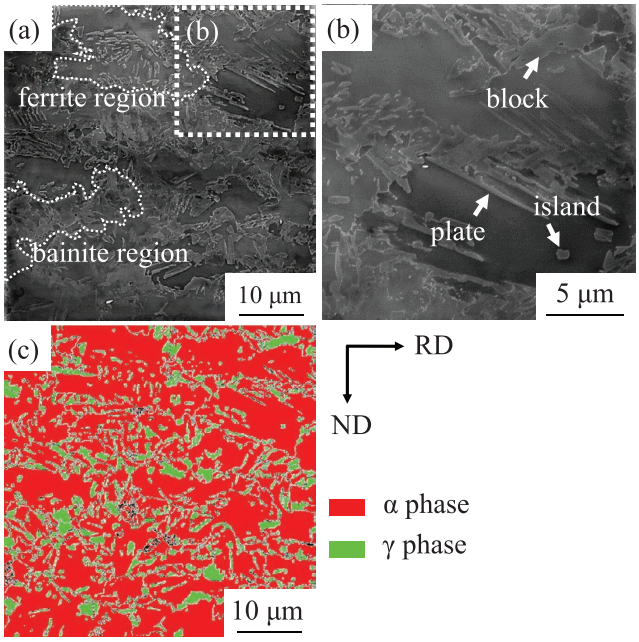

Fig. 3. Microstructure of the test steel on the TD plane: (a) secondary electron image, (b) magnified image of (a), and (c) EBSD phase map of (a). Arrows in (b) indicate three types of retained austenite grains. (Online version in color.)

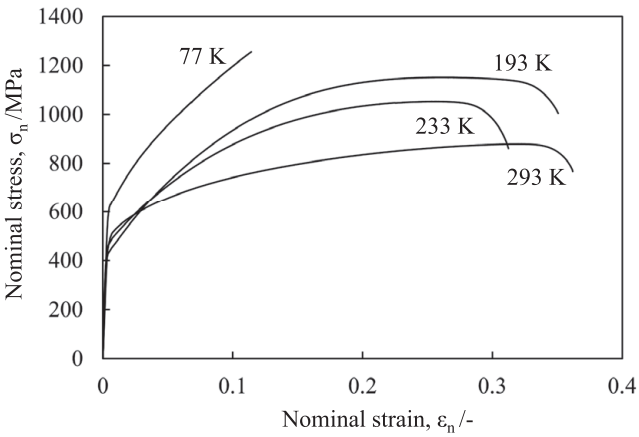

Fig. 4. Nominal stress-strain curves of the test steel at low temperatures.

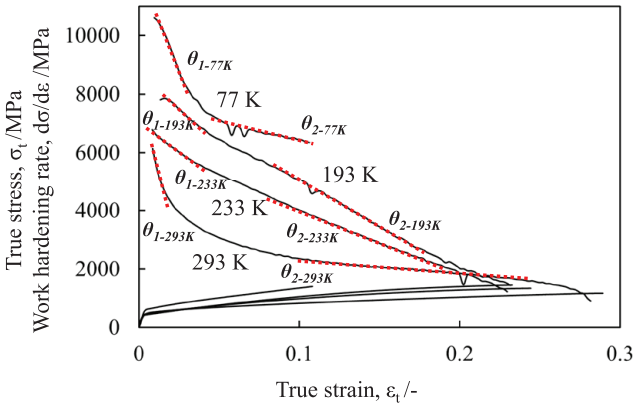

Fig. 5. Work-hardening rate and true stress - true strain curves of the test steel at low temperatures. Dashed lines indicate the tangential components, θ_1 and θ_2, of the work-hardening rate in the initial and final stages. (Online version in color.)

Table 1. Tensile properties of the test steel.

Temperature (K)	0.2% proof stress $\sigma_{0.2}$ (MPa)	Ultimate tensile strength σ_B (MPa)	Total elongation El (%)	Reduction of area RA (%)
293	491	876	36.2	58.4
233	473	1 084	31.2	63.6
193	427	1 152	35.1	43.0
77	625	1 277	10.8	6.2

stage I (easy glide), stage II (linear hardening), and stage III (parabolic hardening).[17] These stages are less evident in polycrystalline steels than in the single crystals.[18] Stage II is an athermal hardening stage that occurs when statistical variations in the dislocation "forest" leads to geometrical storage of dislocations. The steadily decreasing hardening rate observed in Stage III is characterized by the increasing rate of loss of dislocation density due to dynamic recovery. Here the tangential components of the work-hardening rate in the initial (θ_1) and final (θ_2) stages, stage II and stage III, respectively, are indicated at each test temperature in Fig. 5. The rates at 77 K and 293 K, $\theta_{1\text{-}77\,K}$ and $\theta_{1\text{-}293\,K}$, respectively, decrease sharply in the initial stage of plastic deformation (below 0.03 true strain). On the other hand, the rates at 193 K and 233 K gradually decrease through the initial and final stages and are a higher than the rate at 293 K in the strain range up to 0.2, *e.g.* $\theta_{1\text{-}193\,K}$, $\theta_{2\text{-}193\,K}$, $\theta_{1\text{-}233\,K}$ and $\theta_{2\text{-}233\,K}$. This is why the steel exhibited superior strength and ductility at 193 K and 233 K. The work-hardening behavior may depend on the strengthening of the α phase and the stability of the retained austenite at the test temperature, as discussed in the following sections.

3.3. Transformation of Retained Austenite in Tension

Figure 6 shows the relationship between the volume fraction of the retained austenite and the true strain at each test temperature where EBSD phase mapping was used to calculate the volume. The retained austenite was stable during cool down to 193 K, but it partially transformed to martensite (approximately 4% in volume) at 77 K. At 293 K, the retained austenite was stable up to 0.03 strains, while the volume fraction decreased between 0.03 and 0.1 strains. For strains higher than 0.1, the martensitic transformation was not substantial. The volume fraction of retained austenite remained approximately 6% in volume during homogenous deformation until fracture. The retained austenite was mostly transformed to martensite for up to 0.1 strain at 233 K and 193 K. The stability of austenite at 233 K was higher than that at 193 K. At 77 K, almost all retained austenite was transformed to martensite below 0.03 strain due to its low mechanical stability. There was no big difference in the volume fraction of retained austenite between the specimen surface and the interior at 293 K and 193 K, as shown in **Fig. 7**. Here, the volume fraction of retained austenite was evaluated by EBSD measurement for both the specimen surface (cyclically unloaded test) and the specimen interior (interrupted test). The stability of retained austenite at each test temperature was insensitive to the measurement position whether the specimen surface or the interior. Then, we identified the volume fraction of retained austenite on the specimen surface as the volume fraction representing the whole of the specimen in the present study.

Each line of θ'_1 and θ'_2 in Fig. 6, which indicates the tangential components of the volume fraction of the retained austenite, is given in the same range of true strain as θ_1 and θ_2 in Fig. 5. The relationship between the volume fraction of retained austenite and the work-hardening rate, based on these lines is discussed in the following paragraph.

At 293 K, the work-hardening rate in the initial stage, $\theta_{1\text{-}293\,K}$, was remarkably decreased as true strain was increased from 0.01 to 0.02 (as shown in Fig. 5), and hardly any

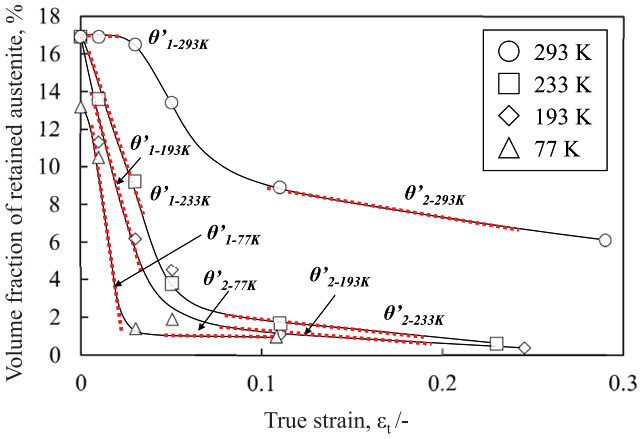

Fig. 6. Volume fraction of the retained austenite after straining at each test temperature. Dashed lines indicate the tangential components, θ'_1 and θ'_2, of the volume fraction of the retained austenite. The lines are given in the same range of true strain as θ_1 and θ_2 in Fig. 5. (Online version in color.)

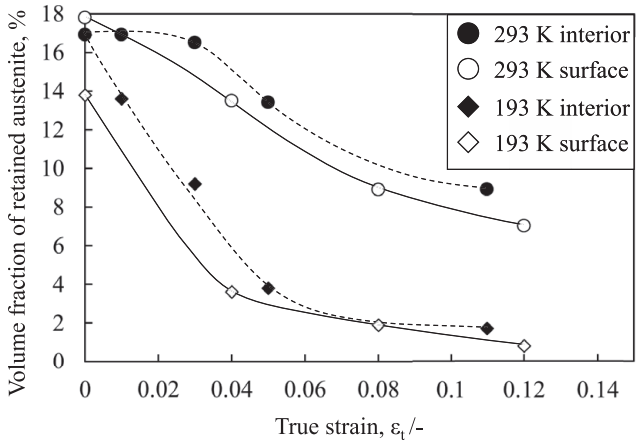

Fig. 7. Volume fraction of retained austenite at the surface and interior of the deformed specimens at 193 K and 293 K.

transformation of the retained austenite to martensite was observed, as can be seen from $\theta'_{1\text{-}293\,K}$ in Fig. 6. Above this strain range, the martensitic transformation of retained austenite sets in, and the work-hardening rate decreases gradually as strain is increased. Although the transformation reduces in the final stage for true strains above 0.1 ($\theta'_{2\text{-}293\,K}$), the work-hardening rate stayed constant as $\theta_{2\text{-}293\,K}$ up to a true strain of 0.25 strain. Since most of the unstable retained austenite transformed to martensite in the initial stage, the remaining austenite may be rather stable mechanically in the final stage. Thus, the retained austenite gradually transformed to martensite, which may maintain the work-hardening rate owing to a dispersed harder phase in the ferrite matrix.

At 233 K and 193 K, the decrease in work-hardening rates with increasing strain in the initial stage is less than that at 293 K ($\theta_{1\text{-}233\,K}$ and $\theta_{1\text{-}193\,K}$), as shown in Fig. 5. In this strain range, the volume of retained austenite was rapidly decreased as indicated ($\theta'_{1\text{-}233\,K}$ and $\theta'_{1\text{-}193\,K}$) in Fig. 6. This is the cause of the increased work-hardening rates. Thereafter the retained austenite was mostly transformed to martensite and the work-hardening rates decrease continuously ($\theta'_{2\text{-}233\,K}$ and $\theta'_{2\text{-}193\,K}$). Therefore, the retained austenite may enhance the work-hardening rate in the initial stage

by means of stress-induced transformation.

At 77 K, the work-hardening rate in the initial stage, $\theta_{I\text{-}77\,K}$, was the highest, as shown in Fig. 5. In the strain range from 0.01 to 0.03, the volume of retained austenite sharply decreases ($\theta'_{I\text{-}77\,K}$ in Fig. 6), and almost all of the retained austenite is transformed to martensite. Thereafter, almost no transformation was detected for higher strains ($\theta'_{2\text{-}77\,K}$), while the work-hardening rate kept gradually decreasing ($\theta_{2\text{-}77\,K}$). Thus, the transformed martensite may induce strain dispersion in the ferrite matrix rather homogeneously.

Therefore, the volume fraction of retained austenite is closely related to the work-hardening rate at each test temperature. Work-hardening rates of the test steel at low temperatures may be enhanced by stress-induced transformation of the retained austenite and strengthening of the ferrite matrix.

3.4. Location and Orientation of Retained Austenite

Figure 8 shows EBSD phase maps overlaid their IQ (image quality) maps under 0.01, 0.03 and 0.1 strains at 293 K, respectively. The IQ maps depict strain as brightness. As demonstrated in a previous study,[8] the α phase of TRIP steel can be distinguished into ferrite and martensite using the IQ parameter.[19] The darker areas indicated by arrows in Fig. 8 correspond to the transformed martensite. Furthermore, the retained austenite in the bainitic region (band-structure) shows a low IQ value, so that the austenite may predominantly transform to martensite. Digital image correlation (DIC) measurements, on the other hand, show that the retained austenite in the high strain regime is mostly transformed into martensite in both the ferrite and bainitic regions. Since the transformation of the retained austenite may depend on its precipitation site and strain distribution around it, the microstructure of the ferrite matrix should also be taken into account for the description of the transformation behavior.

Figure 9 shows orientation maps of retained austenite and their inverse pole figures (IPF) on the interrupted specimen surfaces under 0.01, 0.03 and 0.1 strains at 293 K. The crystal orientation was analyzed along the RD. The highlighted areas (blue color) in Figs. 9(d)–9(f) lie near the zone normal to <111> with a tolerance angle of 15°. The ratio of the number of crystals with said orientation to those with all orientations was determined. The ratio increased from approximately 23% to 39% as strain increased from 0.01 to 0.1. **Figure 10** summarizes the volume ratio of austenite near the zone normal to <100>, <110>, and <111> with a tolerance angle of 15° as a function of strain at each test temperature. The ratio of <111> austenite at the temperatures between 193 K and 293 K was almost the same as for the other orientations up to a strain of 0.05 above which the ratio of <111> austenite increases. Above a strain of 0.1, the value reaches about 40% which appears to be close to saturation. The ratios of <100> and <110> austenite, on the other hand, decrease slightly with an increase in the strain. No change in the ratios among <100>, <110>,

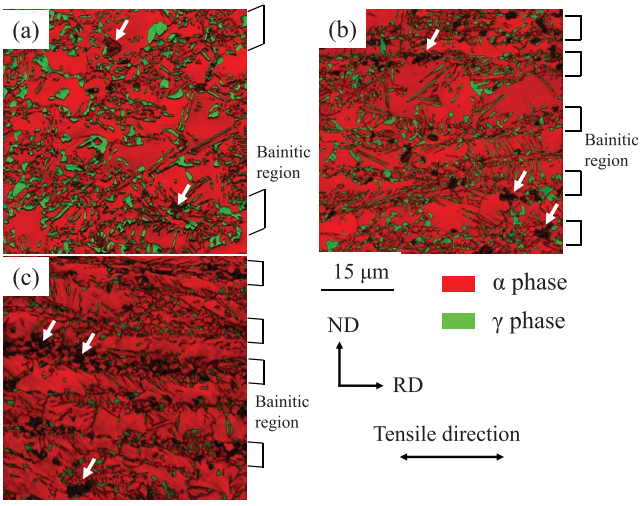

Fig. 8. EBSD phase maps overlaid their image quality maps of the deformed specimens under (a) 0.01 strain, (b) 0.03 strain and (c) 0.1 strain at 293 K. Arrows indicate deformation-induced martensite near bainitic region. (Online version in color.)

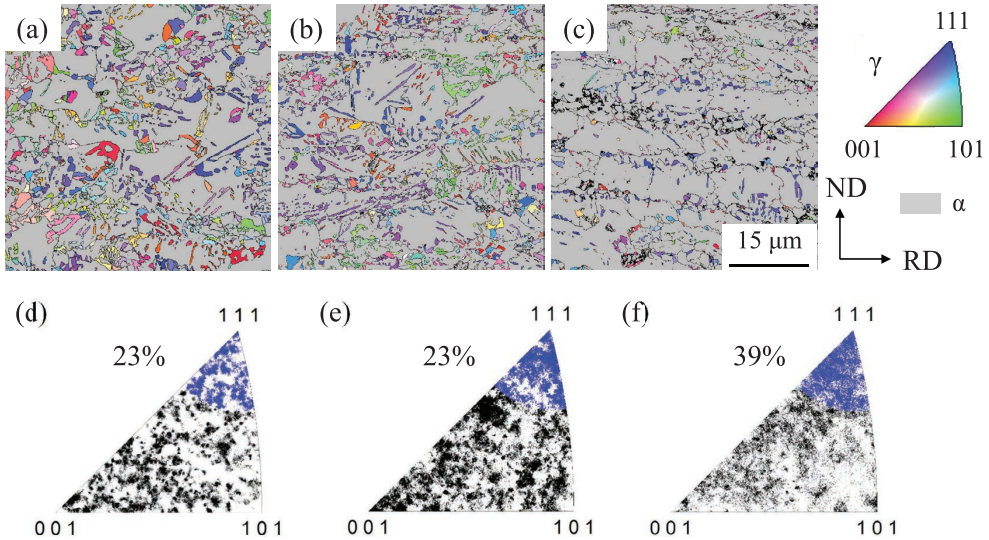

Fig. 9. Orientation maps of retained austenite phase under (a) 0.01 strain, (b) 0.03 strain and (c) 0.1 strain at 293 K. Their inverse pole figures are shown in (d)–(f), respectively. The orientations near the <111> zone normal (tolerance angle of 15°) are highlighted with the ratio. (Online version in color.)

and <111> austenite was detected at 77 K. Furthermore, the orientation analysis at 293 K using neutron diffraction revealed that the <100> and <111> austenite volumes in the steel were relatively high parallel to the RD as shown in **Fig. 11**(a). Figures 11(b) and 11(c) show that above a strain of 0.1, the ratio of <111> austenite was enhanced, while the ratio of <100> austenite was reduced. The highest intensity of <111> retained austenite along the tensile direction after straining agrees with the result obtained by EBSD measurement as well as the result in a previous report involving high-energy X-ray diffraction analysis.[20] The volume ratios of the different orientations of the retained austenite crystals were analyzed by the cyclically unloaded test at 293 K using the same surface area of the specimen surface as for the measurements above. Each point in **Fig. 12** represents the ratio of austenite in each orientation with less than 15° of variance through the test. Namely, the crystal rotation of the retained austenite during straining was eliminated from the data. The volume ratio of <111> austenite increases slightly as a function of true strain, while the ratios of the other two orientations decreases gradually. The volume ratio of <111> austenite was lower only several presents in volume than the ratio indicated in Fig. 10. Therefore, the <111> austenite was mechanically stable at the temperatures between 193 K and 293 K. This suggests that the <111> austenite was hardly deformed and was stable against strain. Thus, not only its mechanical stability but also its deformability may strongly affect the martensitic transformation in the steel. In addition, the austenite grain rotation increased the ratio of <111> austenite. The deformation and crystal rotation of the ferrite matrix may be responsible for the rotation of austenite, since the retained austenite is dispersed in the ferrite matrix. On the other hand, almost all of austenite is transformed into martensite regardless of their orientation at 77 K because of their low phase stability.

3.5. Crystal Rotation of Ferrite Matrix in Tension

As mentioned in the section 3.4, crystal rotation of the ferrite matrix was characterized as shown in **Fig. 13**. The volume ratios of ferrite near the zone normal to <100>, <110>, and <111> with a tolerance angle of 15° were summarized as a function of strain at each test temperature. The ratio of <110> ferrite increased monotonously from approximately 23% to 40% as strain increased from 0.01 to 0.1 for temperatures between 193 K and 293 K. On the other hand, the ratios of <100> and <111> ferrite were gradually decreased with increasing strain. At 77 K, the crystal rotation of the ferrite matrix could hardly be detected under straining.

The retained austenite satisfied the K-S OR with the ferrite matrix after the heat treatment. Even after the tensile tests, this relation with the ferrite matrix still holds, *i.e.* $(111)\gamma//(110)\alpha$. In addition, the volume ratios of both <111> retained austenite and <110> ferrite, which lie parallel to each other, are enhanced. This means that the retained austenite was deformed in accommodative with the deformed ferrite matrix. Therefore, austenite grains are

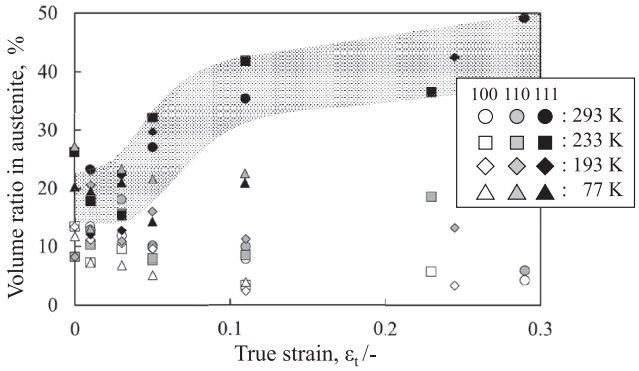

Fig. 10. Volume ratio of retained austenite near the zone normal to <100>, <110> and <111> with a tolerance angle of 15°. Shaded area highlights the increase in the relative ratio of <111> austenite.

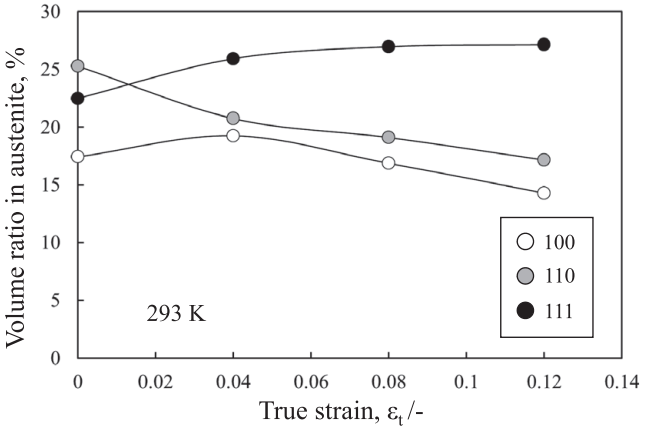

Fig. 12. Volume ratio of retained austenite near the zone normal to <100>, <110> and <111> with a tolerance angle of 15° on the specimen surface without crystal rotation at 293 K.

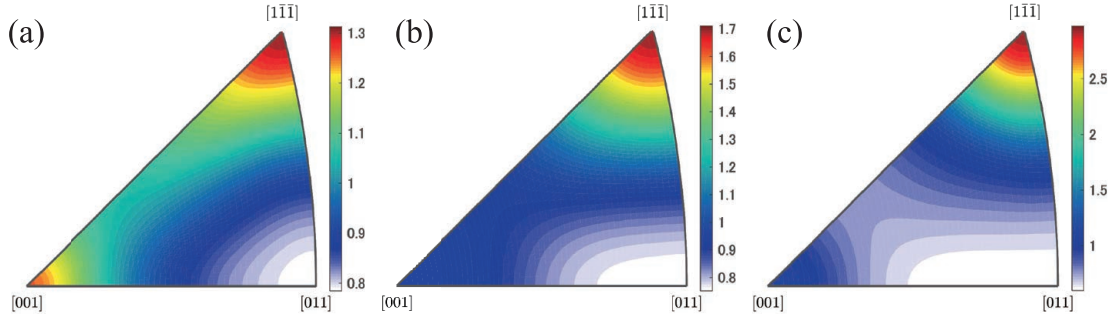

Fig. 11. Orientation of retained austenite normal to RD obtained by neutron diffraction measurements under tension at 293 K: (a) 0 strain, (b) 0.1 strain and (c) 0.29 strain (fracture). (Online version in color.)

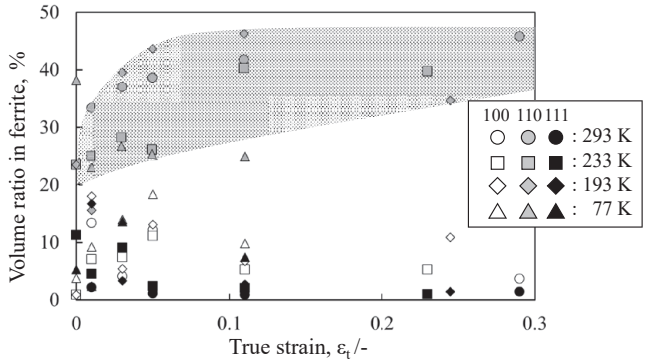

Fig. 13. Volume ratio of ferrite near the zone normal to <100>, <110> and <111> with a tolerance angle of 15°. Shaded area highlights the increase in the relative ratio of <110> ferrite.

rotated to $<111>\gamma$ as stated by the K-S OR with the ferrite matrix rotated to $<110>\alpha$ parallel to the tensile direction in tension.

4. Conclusions

The tensile properties and mechanical stability of retained austenite in a low alloy TRIP steel were evaluated at low temperatures. The main results are summarized as follows:

(1) The test steel showed a good balance of strength and ductility in a temperature range from 193 K to 293 K. A high work-hardening rate in the initial stage of deformation and strengthening of the ferrite matrix by lowering temperature were responsible for the good balance. The higher work-hardening rate at low temperatures may be enhanced by stress-induced transformation of retained austenite.

(2) The retained austenite near the zone normal to <111> was mechanically stable at the temperatures between 193 K and 293 K, since it was hardly deformed compared to the other orientations and was stable against strain. Not only its mechanical stability but also its deformability may strongly affect the martensitic transformation in the steel.

(3) The crystal rotation of ferrite matrix was additionally responsible for the rotation of the dispersed austenite to <111> along the tensile direction where the K-S orientation relationship was satisfied between them.

(4) Almost all of the retained austenite was transformed to martensite regardless of its orientation at 77 K because of its low phase stability.

Acknowledgement

We are grateful to Dr. Y. Onuki of Ibaraki University for his experimental assistance on neutron diffraction experiment at the Materials and Life Science Experimental Facility of the J-PARC. (Proposal No. 2016PM0001).

REFERENCES

1) B. C. De Cooman: *Curr. Opin. Solid State Mater. Sci.*, **8** (2004), 285.
2) I. Tamura: *Tetsu-to-Hagané*, **56** (1970), 429.
3) K. Sugimoto, M. Kobayashi and S. Hashimoto: *Metall. Mater. Trans. A*, **23A** (1992), 3085.
4) A. Itami, M. Takahashi and K. Ushioda: *ISIJ Int.*, **35** (1995), 1121.
5) K. Sugimoto, M. Misu, M. Kobayashi and H. Shirasawa: *ISIJ Int.*, **33** (1993), 775.
6) G. K. Tirumalasetty, M. A. van Huis, C. Kwakernaak, J. Sietsma, W. G. Sloof and H. W. Zandbergen: *Acta Mater.*, **60** (2012), 1311.
7) K. Sugimoto, T. Iida, J. Sakaguchi and T. Kashima: *ISIJ Int.*, **40** (2000), 902.
8) T. Yamashita, N. Koga and O. Umezawa: *Key Eng. Mater.*, **741** (2017), 36.
9) L. Cheng, A. Bottger, Th. H. de Keijser and E. J. Mittemeijer: *Scr. Metall. Mater.*, **24** (1990), 509.
10) Y. Onuki, A. Hoshikawa, S. Sato, T. Ishigaki and T. Tomida: *J. Mater. Sci.*, **52** (2017), 11643.
11) G. Kurdjumov and G. Sachs: *Z. Phys.*, **64** (1930), 325.
12) T. Maki, Y. Tomota and I. Tamura: *J. Jpn. Inst. Met.*, **38** (1974), 871.
13) A. Narui, S. Chen, Y. Tomota and T. Kamiyama: *Trans. Jpn. Soc. Mech. Eng. A,* **75A** (2009), 501.
14) K. Sugimoto, N. Usui, M. Kobayashi and S. Hashimoto: *ISIJ Int.*, **32** (1992), 1311.
15) G. R. Speich, V. A. Demarest and R. L. Miller: *Metall. Trans. A*, **12A** (1981), 1419.
16) J. B. Gilmour, G. R. Purdy and J. S. Kirkaldy: *Metall. Trans.*, **3** (1972), 1455.
17) D. Kuhlmann-Wilsdorf: *Metall. Trans. A*, **16A** (1985), 2091.
18) R. E. Reedhill, W. R. Cribb and S. N. Monteiro: *Metall. Trans.*, **4** (1973), 2665.
19) E. P. Kwon, S. Fujieda, K. Shinoda and S. Suzuki: *Mater. Sci. Eng. A*, **528** (2011), 5007.
20) R. Blondé, E. Jimenez-Melero, L. Zhao, J. P. Wright, E. Brück, S. van der Zwaag and N. H. van Dijk: *Acta Mater.*, **60** (2012), 565.